JGR Atmospheres

RESEARCH ARTICLE
10.1029/2025JD044843

Fine Tuning Eruption Source Parameters to Improve Ash Dispersion Simulations: An Example From Eyjafjallajökull 2010

F. Dioguardi[1,2], S. Corradini[3], T. Dürig[4,5], L. Guerrieri[3], L. Merucci[3], and D. Stelitano[3]

[1]Dipartimento di Scienze della Terra e Geoambientali, University of Bari "Aldo Moro", Bari, Italy, [2]The Lyell Centre, British Geological Survey, Edinburgh, UK, [3]Osservatorio Nazionale Terremoti, Istituto Nazionale di Geofisica e Vulcanologia, Rome, Italy, [4]Institute of Earth Sciences, University of Iceland, Reykjavik, Iceland, [5]Now at Federal Criminal Police Office (BKA), Forensic Science Institute, Wiesbaden, Germany

Key Points:

- Improved time series of eruption source parameters (ESPs) (top plume height and mass eruption rate) of the Eyjafjallajökull 2010 test case
- Volcanic ash mass loadings in the atmosphere were modeled with FALL3D and compared with satellite-retrieved ones
- Results showed that the improved ESPs lead to a significantly better match with satellite retrievals

Supporting Information:

Supporting Information may be found in the online version of this article.

Correspondence to:

F. Dioguardi,
fabio.dioguardi@uniba.it

Citation:

Dioguardi, F., Corradini, S., Dürig, T., Guerrieri, L., Merucci, L., & Stelitano, D. (2025). Fine tuning eruption source parameters to improve ash dispersion simulations: An example from Eyjafjallajökull 2010. *Journal of Geophysical Research: Atmospheres*, *130*, e2025JD044843. https://doi.org/10.1029/2025JD044843

Received 16 JUL 2025
Accepted 22 NOV 2025

Author Contributions:

Conceptualization: F. Dioguardi, T. Dürig
Data curation: F. Dioguardi, S. Corradini, T. Dürig, L. Guerrieri, L. Merucci, D. Stelitano
Formal analysis: F. Dioguardi, S. Corradini, T. Dürig, L. Guerrieri
Investigation: F. Dioguardi, S. Corradini, T. Dürig, L. Guerrieri, L. Merucci, D. Stelitano
Methodology: F. Dioguardi, T. Dürig
Resources: F. Dioguardi
Software: F. Dioguardi, S. Corradini, L. Guerrieri, L. Merucci, D. Stelitano

Abstract Volcanic ash dispersion simulations and remote sensing of ash clouds are conducted by volcano observatories and Volcanic Ash Advisory Centres to monitor and forecast the evolution of volcanic ash clouds in space and time in order to mitigate the risk posed by these events on civil aviation. Despite constant improvements in terms of technology and modern capabilities, both numerical simulations and monitoring are still affected by variable degrees of uncertainty. To initialize the rate of emission and position of the volcanic ash in the ash dispersion simulation computational domain of the numerical model used for forecasting the ash clouds, in particular, currently relies on the preliminary simulation of the volcanic plume. The source modeling is generally carried out using simplified plume models that depends on parameters that cannot be accurately measured in real time, for example, the wind entrainment coefficient and the plume centerline height in case of wind affected (bent-over) plumes. In this work, we test recently proposed correction factors for these parameters for two of the most widely used simplified plume models and compare with ash cloud satellite observations retrieved during the Eyjafjallajökull eruption. Specifically, we compare modeling results obtained with and without applying the corrections of the top plume height and wind entrainment coefficient. We show that, by applying the corrections, we significantly reduce the discrepancy between the simulated and satellite-retrieved ash cloud observations.

Plain Language Summary Explosive volcanic eruptions are responsible for the injection of volcanic ash into the atmosphere. Volcanic ash clouds represent a threat for civil aviation, and therefore a great effort has been made in order to improve the observation and forecasting of these clouds. Recent studies have shown that the estimation of the mass of ash released into the atmosphere over time, which is done by applying simplified models, can be improved by fine-tuning some parameters that can be estimated in near real time. In this work we show, by comparing results of ash dispersion modeling and satellite retrievals of the Eyjafjallajökull 2010 eruption, how this improvement results in a closer match between the simulated and observed ash cloud.

1. Introduction

Volcanic ash atmospheric dispersion modeling and remote sensing observation of the ash in the atmosphere are fundamental tools for Volcanic Ash Advisory Centres (VAAC) (VAACs) to monitor and forecast the spatial and temporal evolution of volcanic ash clouds and tephra sedimentation over the ground. This is an important task, since volcanic ash in the atmosphere can be harmful to aircraft engines and, therefore, potentially disruptive for the aviation industry (Durant et al., 2010; Giehl et al., 2017; Grindle & Burcham, 2002; Kienle et al., 1980). Therefore, a significant effort has been made to improving our observational and modeling capabilities of the volcanic ash cloud and the plume, which are the processes responsible for the injection of ash in the atmosphere. The volcanic plume and ash cloud monitoring and modeling, which are linked to each other, need to be carried out quickly during volcanic crises, which is why testing the observational and modeling procedures in VAACs and volcano observatories represent best practices (Beckett et al., 2024).

Atmospheric ash dispersion and deposition modeling is currently mostly conducted in two successive steps:

Supervision: F. Dioguardi, T. Dürig
Validation: F. Dioguardi, S. Corradini, L. Merucci, D. Stelitano
Visualization: F. Dioguardi
Writing – original draft: F. Dioguardi, S. Corradini, L. Guerrieri, L. Merucci, D. Stelitano
Writing – review & editing: F. Dioguardi, S. Corradini, T. Dürig, L. Guerrieri, L. Merucci, D. Stelitano

- Ash emission modeling, normally using eruption source parameters (ESPs) (mass flux or MER, top plume height (h), total grainsize distribution (TGSD), etc.) either from available data sets (e.g., Aubry et al., 2021) or estimated via plume models;
- Atmospheric dispersion and sedimentation modeling using various modeling approaches spanning from particle tracking or Lagrangian (e.g., NAME, Beckett et al., 2020; Jones et al., 2007) to solving the advection-diffusion-sedimentation equation or Eulerian (e.g., FALL3D, Costa et al., 2006; Folch et al., 2020) to hybrid approaches (e.g., HYSPLIT, Stein et al., 2015).

Both steps require meteorological data, generally coming from Numerical Weather Prediction models. This procedure is affected by uncertainty propagation from the emission to the dispersion modeling (e.g., Dioguardi et al., 2020). Although currently available atmospheric dispersion and sedimentation models like NAME and FALL3D allow modeling both steps at once, the coupling between the processes and the meteorology is always "offline," that is, the emission of ash is modeled first and without affecting the atmospheric conditions, followed by the solution of the atmospheric dispersion of ash. Marti et al. (2017) presented an "online" coupling of the second (dispersion and sedimentation modeling) step, but the first step was kept offline. Recently, though, some efforts have been made towards "online" coupling (e.g., Bruckert et al., 2022; Rizza et al., 2020, 2023), but these methodologies based on complex and computationally demanding approaches cannot be used for operational applications due to the currently available computational capabilities and required runtime. This is why the aforementioned steps-based methodology is still widely used and a great deal of research is still being dedicated to the improvement of both plume and atmospheric dispersion models.

The generation of a volcanic plume is the most common process responsible for the injection of tephra into the atmosphere (e.g., Sparks et al., 1997; Wilson & Walker, 1987; Woods, 1988). The MER and h are, together with meteorological conditions, the two main parameters used to quantitatively characterize the volcanic plume and to initialize the subsequent dispersion simulation. h can be obtained by remote sensing observations like ground based cameras (Guerrieri et al., 2025; Scollo et al., 2014), radars (Corradini et al., 2016), thermal infrared signatures (e.g., Birnbaum et al., 2023; Valade et al., 2014) or satellites (Corradini et al., 2018; de Michele et al., 2019; Guerrieri et al., 2023; Merucci et al., 2016; Prata & Grant, 2001). MER, on the other hand, is much more difficult to measure in real time although some progress has been made recently, for example, using video analyses of ash plumes and ejecta (Dürig et al., 2015a, 2015b; Pioli & Harris, 2019; Tournigand et al., 2019; Valade et al., 2014; Wilson & Self, 1980), thermal infrared signatures (Cerminara et al., 2015; Harris, 2013; Harris et al., 2013; Ripepe et al., 2013), emitted infra-sound waves (Johnson & Ripepe, 2011; Ripepe et al., 2013), electrostatic field (Büttner et al., 2000; Calvari et al., 2012), interpretation of microwave radar signals (Marzano et al., 2020; Montopoli, 2016) or integration between ground based and satellite sensors (Freret-Lorgeril, Bonadonna, Corradini, Donnadieu, et al., 2021; Freret-Lorgeril, Bonadonna, Corradini, Guerrieri, et al., 2021). However, these methodologies are affected by large uncertainties when applied to real-time assessments, since they are based on parameters that are either unknown or difficult to estimate during an eruption (e.g., the vent geometry as in Dürig et al. (2015a)). For this reason, currently MER is more commonly indirectly estimated using plume models linking h to MER.

There are several plume models available, ranging from simple equations linking h to MER which can be either empirical, based on ESPs databases (Aubry et al., 2023; Gudmundsson et al., 2012; Mastin et al., 2009; Sparks et al., 1997) or analytical (Degruyter & Bonadonna, 2012; Wilson & Walker, 1987; Woodhouse et al., 2013; Woods, 1988), to more complex models based on the conservation equations of fluid dynamics. The former are usually classified as "0D" models. The latter in turn can be simplified to steady 1D homogeneous models (e.g., Bursik, 2001; Degruyter & Bonadonna, 2012; de' Michieli Vitturi et al., 2015; Devenish, 2013; Folch et al., 2016; Mastin, 2014; Woodhouse et al., 2013), unsteady 1D homogeneous models (e.g., Dürig et al., 2015a, 2015b; Hochfeld et al., 2022; Scase & Hewitt, 2012; Woodhouse et al., 2016), and more complex time-dependent multiphase models (e.g., Cerminara et al., 2016; Esposti Ongaro et al., 2007; Suzuki & Koyaguchi, 2012). 0D models are the most widely used to estimate the MER in real-time operational applications, because they are fast and require few input parameters that can be generally obtained easily, although 1D models are also being employed, for example, in the Icelandic Met Office VESPA system (http://brunnur.vedur.is/radar/vespa), which implements the model of de' Michieli Vitturi et al. (2015). The accuracy of 0D models depends on the eruptive style (e.g., sustained versus unstable eruptive column, the former being a better scenario for these models) and meteorological conditions, in particular related to the eruptive column evolution itself (e.g., strong versus weak bent-over plume). In fact, these models can (e.g., Degruyter & Bonadonna, 2012; Woodhouse et al., 2013) or cannot (Aubry

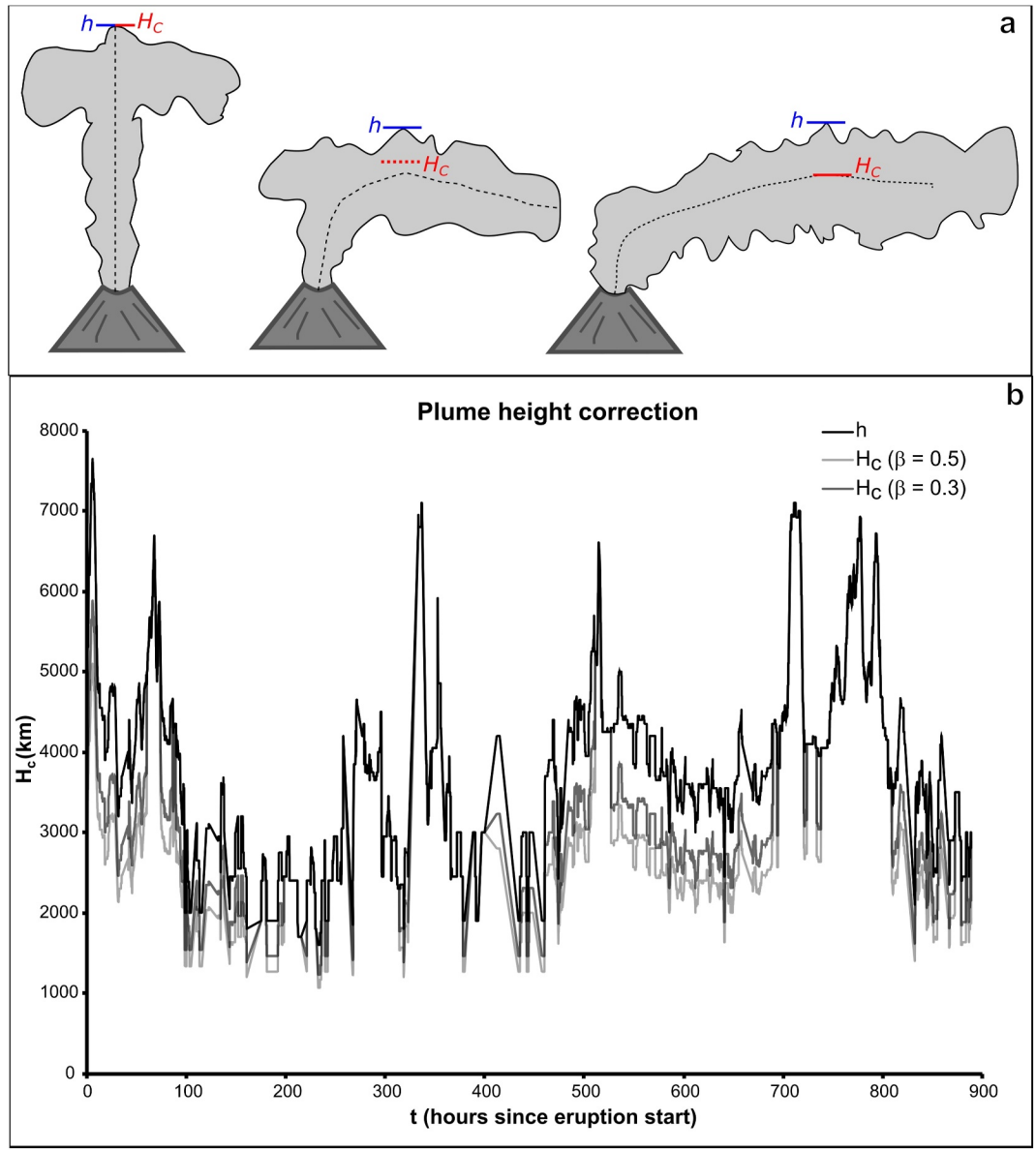

Figure 1. (a) Top plume height h versus top centerline height H_c in three scenarios: strong, intermediate, and weak plume (from the left to the right). Modified after Dürig et al. (2023b); © 2023. American Geophysical Union. All Rights Reserved. (b) Top plume height h (black line) and top centerline height H_c time series; the latter are obtained with $\beta = 0.5$ (light gray line) and $\beta = 0.3$ (dark gray line).

et al., 2023; Gudmundsson et al., 2012; Mastin et al., 2009; Sparks et al., 1997; Wilson & Walker, 1987; Woods, 1988) take the effect of wind into account, and consequently it was shown that certain models might provide more accurate predictions under specific conditions than others (Aubry et al., 2023; Dioguardi et al., 2020; Dürig et al., 2018, 2023a). Furthermore, wind-affected 0D models require a h correction since they relate MER to the top centerline height H_c, which is challenging to obtain with currently used monitoring technologies (Figure 1a). Finally, all 0D models strongly depend on the atmospheric air entrainment parametrization, for which there is no consensus especially for the entrainment caused by the action of wind.

The 2010 eruption of Eyjafjallajökull volcano (hereafter referred to as Eyja2010), by means of the disruption that it caused to various sectors (Harris et al., 2012), triggered a probably unprecedented research and infrastructural effort targeted at improving the observational, modeling and response capabilities during explosive volcanic eruptions. The eruption was characterized almost constantly by a weak (bent-over) plume, from which ash was

advected towards the south during most of its duration. Arason et al. (2011) published the complete record of h obtained from the C-band radar based in Keflavík airport. Dürig et al. (2023b), by using this data set and, when possible, pictures of the plume, showed that the performance of 0D plume models, in particular the wind-affected ones, could be improved by applying corrections to h in order to estimate the H_c and, specifically for Eyja2010 case, by a different formulation of the wind entrainment parametrization.

In this work we first review the wind-affected 0D models and the improvements proposed by Dürig et al. (2023b) to obtain a more accurate time series of MER versus H_c for the whole Eyja2010 eruption. We then compare the FALL3D atmospheric ash dispersion outputs obtained with the original and improved MER versus H_c time series with ash column loading data extrapolated from satellite imagery.

2. Materials and Methods

In order to show the impact of the modified ESPs time series following the prescriptions in Dürig et al. (2023b) on the predicted ash clouds, we:

- created a new time series of the ESPs by using (a) the plume model of Degruyter and Bonadonna (2012) and (b) the model of Woodhouse et al. (2013);
- carried out atmospheric dispersion simulations using the original and the modified ESPs by means of FALL3D (Folch et al., 2020);
- compared simulated with observed ash column loadings.

In the following we go into the details of these methodological steps.

2.1. The Corrected Plume Height and Mass Eruption Rate Time Series of the Eyjafjallajökull 2010 Eruption

Eyjafjallajökull is a volcano in southern Iceland, whose summit is at 1,666 m above sea level and covered by ice (Jonsson, 1988; Sæmundsson, 1979). The details of the Eyja2010 eruption can be found in Dellino et al. (2012) and Gudmundsson et al. (2012). The eruption consisted of three phases: the first one (14–18 April) produced a plume rising to 5–10 km high alternating between dark gray (loaded with tephra) and some steam-rich plumes. The second phase (18 April–4 May) was characterized by mainly lava effusion and much weaker explosive activity. The third phase (5–17 May) saw an increase in explosive intensity before a final phase of decline (18–22 May). During most of the eruption, from the volcanological point of view the volcanic plume was "weak" since it was generally bent-over by the wind. Given the almost constant "weak plume condition," in order to quantitatively address this interaction with the wind, Dürig et al. (2023b) estimated the plume type parameter Π (Degruyter & Bonadonna, 2012), which quantifies the relative influence of buoyancy and cross-wind on the plume dynamics, for the whole duration of the eruption:

$$\Pi = \frac{\overline{N}h}{1.8 \cdot \overline{v}} \cdot \left(\frac{\alpha}{\beta}\right)^2 \tag{1}$$

Table 1 lists all the symbols used in this manuscript, the upper bar $\overline{\ }$ denotes the depth averaging across the plume height. In Equation 1, $\overline{N}$ is the plume height-averaged buoyancy frequency (N), h is the top plume height, $\overline{v}$ is the plume height-averaged wind speed (v), α and β are the radial and wind entrainment coefficients, respectively. $\overline{N}$ is defined as:

$$\overline{N}^2 = \frac{1}{H_C}\int_0^{H_C} N^2(z)\,dz = \frac{1}{H_C}\frac{g}{c_{a0}T_{a0}}\int_0^{H_C}\left(1 + \frac{c_{a0}}{g}\frac{dT_a}{dz}\right)dz \tag{2}$$

where H_c is the top plume centerline height, z is the vertical coordinate, c_a and T_a are the specific heat capacity and temperature of the air, g is the gravitational acceleration, and the subscript 0 refers to the volcanic vent height (the height of the plume source). Large values of Π are expected for strong (not wind affected) plumes, whilst very low values of Π characterize weak (wind affected) plumes. Different thresholds values for these scenarios, including intermediate plumes in between, have been proposed in the literature. For example, Bonadonna et al. (2015)

Table 1
Symbols List

Symbol	Meaning	Units
Π	Plume type parameter	–
$\Delta A\%$	Percent difference ($\Delta A\%$) of the area A of the ash cloud where ML > 0.5 g m^{-2} between the reference and test solution	–
$\widetilde{W_s}$	Wind shear parameter	–
A	Area of the domain covered by the ash cloud	km^2
c	Specific heat capacity	J kg^{-1} K^{-1}
C	Particle volumetric concentration	–
C	Ash mass concentration	mg m^{-3}
g	Gravitational acceleration	m s^{-2}
g'	Reduced gravity	m s^{-2}
h	Top plume height	m
H_c	Top plume centerline height	m
MER	Mass eruption rate	kg s^{-1}
ML	Particle column mass loading	g m^{-2}
ML$_{sat}$	Satellite retrieved-particle column mass loading	g m^{-2}
ML$_{sim}$	Simulated particle column mass loading	g m^{-2}
N	Buoyancy frequency	s^{-1}
r	Plume centerline height correction factor	–
T	Temperature	K
V	Volume of the domain covered by the ash cloud	km^3
v	Wind speed	m s^{-1}
z	Vertical coordinate	m
α	Radial entrainment coefficient	–
β	Wind entrainment coefficient	–
ρ_{a0}	Air density at the plume vent height	kg m^{-3}

defined weak and strong plumes by $\Pi < 0.1$ and $\Pi > 10$, respectively, with transitional plumes in between. Scollo et al. (2019) revised the upper threshold value reducing it to 0.5. More recently, Dürig et al. (2023b), by means of the software Real-time ESPs FutureVolc Information and Reconnaissance system (REFIR, Dürig et al., 2018) and the top plume height data recorded during the Eyjafjallajökull 2010 eruption by the C-band radar installed in Keflavík (Arason et al., 2011), showed that the eruptive plume could be classified as weak or intermediate over the whole eruption duration based on Scollo's threshold values. Consequently, in this study we focused on the simplified wind-affected plume models of Degruyter and Bonadonna (2012) (hereafter referred to as DBM, Equation 3) and Woodhouse et al. (2013) (hereafter referred to as WM, Equation 4):

$$\mathrm{MER}_{\mathrm{DBM}} = \pi \frac{\rho_{a0}}{g'} \left(\frac{2^{5/2} \alpha^2 \overline{N}^3}{{z_1}^4} {H_C}^4 + \frac{\beta^2 \overline{N}^2 \overline{V}}{6} {H_C}^3 \right) \tag{3}$$

$$\mathrm{MER}_{\mathrm{WM}} = \left(\frac{1}{0.318} H_C \frac{1 + 4.266 \widetilde{W_s} + 0.3527 \widetilde{\widetilde{W_s}}^2}{1 + 1.373 \widetilde{\widetilde{W_s}}} \right)^{3.953} \tag{4}$$

which calculate the MER at the plume source as a function of the top centerline height. In Equation 3 ρ_{a0} is the air density at the plume source elevation, g' is the reduced gravity defined as:

$$g' = g\frac{c_0T_0 - c_{a0}T_{a0}}{c_{a0}T_{a0}} \quad (5)$$

In which c_0 and T_0 are the bulk specific heat capacity and temperature of the plume at the source. In Equation 4 $\widetilde{W}_s$ is a parameter quantifying the wind shear across the plume from the source to a reference height H_1:

$$\widetilde{\widetilde{W}}_s = 1.44\frac{v_1}{\overline{N}H_1} \quad (6)$$

in which v_1 is the wind speed at the reference height H_1, which is taken equal to H_c in Woodhouse et al. (2013). In these wind affected models it is evident how the wind plays a significant role in the calculation of MER, specifically by increasing the predicted MER with increasing wind speed v (see Figure 4 of Dioguardi et al. (2020)).

The complete time series of top plume height data of Arason et al. (2011), which covers the whole Eyja2010, was processed with REFIR, a software that computes the best estimate of top plume heights (retrieved from various possible sources) and MER using simplified plume models (including DBM and WM). Specifically, we set with a time base of 30 min (see Dürig et al. (2018) and Dioguardi et al. (2020) for further details) in order to obtain a reliable time series of top plume centerline height H_c following one of the approaches discussed in Dürig et al. (2023b), namely the "Theoretical centerline correction," which is based on the Devenish (2016) model. Specifically, when condition $\Pi < 0.1$ is satisfied (weak plume), the top plume height is reduced by a factor r such as:

$$H_c = h(1 - r) \quad (7)$$

$$r = \frac{\beta}{1 + \beta} \quad (8)$$

Otherwise no correction is applied, therefore the top plume centerline height H_c coincides with the top plume height h.

The original h time series recorded by the C-band radar in Keflavík has a time resolution of 5 min; some gaps in the recordings were corrected by simple linear interpolation as in Folch et al. (2012) and Dioguardi et al. (2020); finally we created a 1 hr-time averaged time series of top plume height, which we used in the subsequent analysis. Dürig et al. (2023b) used REFIR (Dürig et al., 2018) to calculate the complete time series of MER (using DBM and WM) starting from the top plume height data; subsequently they calculated the total erupted mass of tephra of the whole eruption and four stages originally identified by Gudmundsson et al. (2012), who computed the MER of these stages starting from the estimation of the total emitted volume from the isopach (deposit thickness) maps and then, from the tephra density, obtaining the total erupted mass of each stage. By comparing simulated versus estimated erupted mass, Dürig et al. (2023b) iteratively searched for the values of β, hence the plume height correction factor r, that resulted in the best match; furthermore, in some cases the latter factor could be directly estimated by photos taken during the eruption showing the bent-over plumes. By combining results of the two approaches, they found that the best results could be obtained with the following combinations:

- DBM: $\beta = 0.3$, which results in $r = 0.23$
- WM: $\beta = 0.5$, which results in $r = 0.33$

It is worth noting that WM does not allow for varying β, since this model comes from the application of Woodhouse et al. (2013) 1D plume model with $\beta = 0.9$; therefore, the prescription above refers to the calculation of r only; on the other hand, the prescription for DBM applies both to the β in the model and r.

Figure 1b shows the time series of h and H_c, the latter obtained after the corrections listed above.

From Figure 1b it is possible to observe that there are some periods in which no correction is applied, that is, H_c coincides with h when $\Pi > 0.1$, in agreement with Dürig et al. (2023b). In the other time intervals the difference between h and H_c is evident and increases with increasing β as expected by the β-dependent values of the correction factor r.

Table 2
IDs and Corresponding Parameters of the Simulations

Test name	Simulation ID	MER model	Wind entrainment coefficient	Radius correction
test_DBM	DBM_original	DBM	$\beta = 0.5$	–
	DBM_modified	DBM	$\beta = 0.3$	$r = 0.23$
test_WM	WM_original	WM	$\beta = 0.9$	–
	WM_modified	WM	$\beta = 0.9$	$r = 0.33$

The meteorological data necessary to use DBM and WM were retrieved by REFIR from the ERA5 reanalysis data set (Hersbach et al., 2018a, 2018b), interpolated onto the eruption location.

2.2. Ash Dispersion Simulations

The atmospheric dispersion of the ash emitted during Eyja2010 was simulated using the FALL3D model (v9.0.2, Folch et al., 2020). FALL3D solves the advection-diffusion-sedimentation equation to simulate the atmospheric passive transport and deposition of solid particles (e.g., ash) and gases.

The simulations were carried out for the whole eruption duration (893 hr starting from the 14 April 2010) with 1-hr time steps on a domain defined as:

- Latitude: from 40°N to 70°N
- Longitude: from 30°W to 10°E
- Vertical coordinate: from 0 to 15,000 m a.s.l.

We discretized the domain with a regular horizontal spacing with a resolution of 0.25°. The vertical spacing follows the linear decay (Folch et al., 2020) with 100 points. We used ERA5 meteorological data with a time step of 1 hr (Hersbach et al., 2018a, 2018b) to run the dispersion simulations. The horizontal turbulent diffusion was modeled using the Byun and Schere (2006) Community Multiscale Air Quality scheme, whilst for the vertical diffusion we used the similarity theory (Neale et al., 2010). The emission source was modeled by approximating the plume with the top-hat geometry, hence ash was emitted along a uniform profile between the top height elevation H_c as derived in Section 2.1 and the vent height. Concerning the emitted particles, we considered only the ash fractions <20 μm diameter with the size fractions taken from Bonadonna et al. (2011) in order to focus only on the particles that could be retrieved from the satellites (Corradini et al., 2011; Wen & Rose, 1994; Yu et al., 2002). Particles' density was set to 2,600 kg m^{-3} whilst their shape was taken as spherical for simplicity. In FALL3D, the shape plays a role in the calculation of the settling velocity; assuming a spherical shape could lead to an overestimation of the terminal velocity, hence the rate at which particles leave the ash cloud, however this effect is minimum to negligible for very small particles settling at low Reynolds number (e.g., Dioguardi et al., 2018).

We carried out the following two tests (Table 2):

The radius corrections (r) were obtained using Devenish (2016) formula.

Figure 2 shows an example of the FALL3D simulated total volcanic ash column mass loading ML_{sim} (ash concentration integrated from the ground to the top of the domain, g m^{-2}) obtained in test_DBM at the same time step (+30 hr from the eruption simulation start at 14 April 2010 00Z) with the original (WM_original, Figure 2a) and modified (WM_modified, Figure 2b) ESPs time series. For the shown time step, the difference between the two simulations is visually evident.

In the following sections we present the data analysis procedure and the results in detail.

2.3. Satellite Retrievals

Two different volcanic ash retrieval procedures have been applied to Moderate Resolution Imaging Spectroradiometer (MODIS) measurements. MODIS aboard the NASA Terra and Aqua polar satellites, acquire data in 36 bands from visible (VIS) to thermal infrared (TIR), with a spatial resolution of 1 km^2 at nadir and a repetition cycle of 1–2 days (http://modis.gsfc.nasa.gov/). The TIR channels 31 and 32 (centered around 11 and 12 μm) are

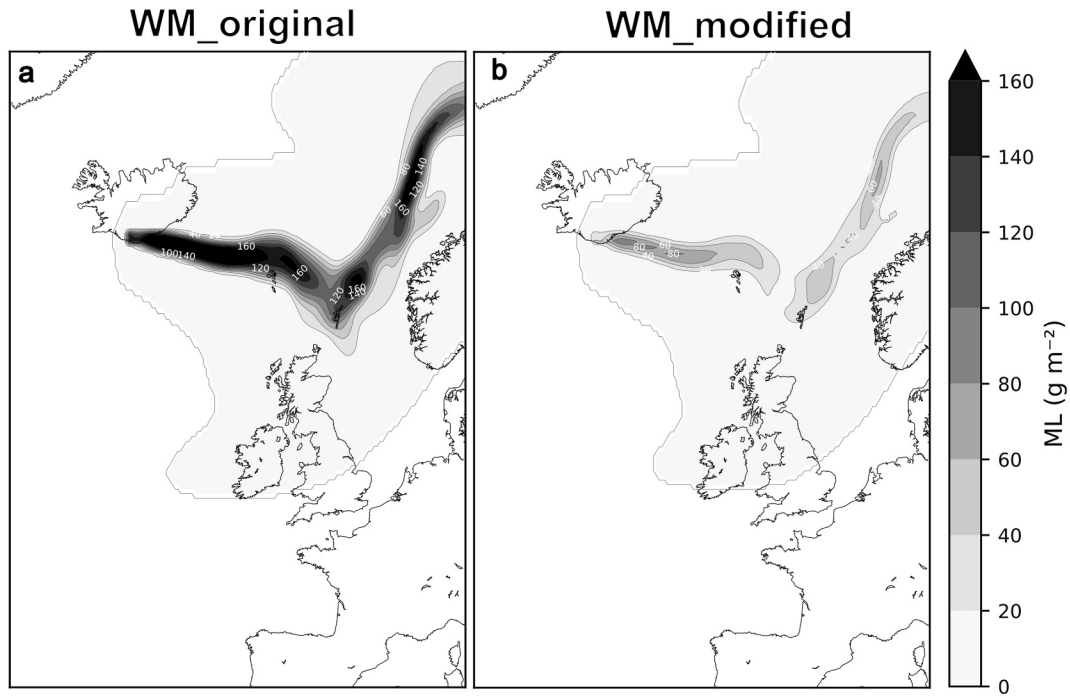

Figure 2. Example of simulated total column ash loading of volcanic ash ML_{sim} obtained with the (a) original (WM_original) and (b) modified (WM_modified) eruption source parameters time series at +30 hr from the simulated eruption start.

used for the volcanic ash mass, aerosol optical depth (AOD) and effective radius (Re) retrievals. Three hundred ten MODIS images have been processed from the start of the Eyjafjallajökull 2010 eruption (16 April) to the end of activity (10 May).

The first approach named Look Up Table procedure (LUT_p) is based on the exploitation of the spectral ash characteristics around 11 and 12 μm (Prata, 1989) and the computation of the inverted arches curves Brightness Temperature Difference versus Brightness Temperature at 11 μm ($T_{b,11}$) (Corradini et al., 2008; Prata & Grant, 2001; Wen & Rose, 1994; Yu et al., 2002). The curves are obtained by running a Radiative Transfer Model (RTM) considering specific atmospheric profiles, volcanic cloud geometry, surface parameters, ash type and varying the volcanic ash cloud AOD and Re. Each ash pixel, identified in the MODIS image, is characterized by an unique couple of BTD-$T_{b,11}$ values that, inserted in the inverted arches plot and through a bilinear interpolation, allows the computation of AOD and Re. From these parameters, the ash mass is obtained by applying the Wen and Rose (1994) simplified formula by considering an ash density of 2,600 kg m^{-3}.

The second procedure (Volcanic Plume Retrieval-VPR, Guerrieri et al., 2015; Pugnaghi et al., 2013, 2016) is a simplified approach based on a linear interpolation of the MODIS radiances surrounding the detected volcanic cloud in order to compute the radiances that would have been measured in the absence of the volcanic cloud. The new image and the original data allow the computation of the volcanic cloud transmittance in the TIR channels centered at 11 and 12 μm by applying a simplified model consisting of a cloud at a constant altitude, temperature, and thickness. The transmittances are then refined with a polynomial relationship obtained by means of RTM simulations adapted for the geographical region, ash type, and atmospheric profiles. From the 11 and 12 μm transmittances the ash parameters can be obtained.

Both retrieval procedures are extensively validated (Corradini et al., 2010, 2014, 2021) and present advantages and drawbacks. In particular, the main advantage of LUT_p is the precise characterization of the scene, but cannot be used in real time (e.g., from VAAC) since fast and reliable interpretations are not possible, while VPR is based on a simplified volcanic cloud model and defined atmospheric parameters but it requires as input only the volcanic cloud altitude and temperature and can be used in real time. The ash abundance uncertainty in the vertical column, for both procedures, has been considered equal to 40% of the retrieved value (Corradini et al., 2008).

3. Data Processing

Both the simulation outputs and the satellite retrievals data are in NetCDF format, therefore the whole data processing discussed below has been carried out by using the Python module netCDF4. The Python codes used for the data processing are provided in the Zenodo data repository (Dioguardi, 2025a). The data analysis was carried out for the whole simulation duration (893 time steps).

We conducted two types of analysis:

1. For each test (Table 2), comparison between the results of the simulations obtained with the original and modified time series of ESPs. Specifically, we calculated the following parameters for the 893 time steps:
   a. The area of the ash cloud where $ML_{sim} > 0.5$ g m^{-2}, which is the satellite detection threshold;
   b. The percent difference ($\Delta A\%$) of the area A of the ash cloud where $ML_{sim} > 0.5$ g m^{-2} between the two simulations' (original and modified) outputs for the two tests;

$$\Delta A\% = \frac{A_{\text{modified}} - A_{\text{original}}}{A_{\text{original}}} * 100 \tag{9}$$

   c. The volume of the domain in which the ash mass concentration (mg m^{-3}) is above the threshold values identified by the International Civil Aviation Organization (ICAO) to be medium (2 mg m^{-3}) and very high (10 mg m^{-3}) (ICAO, 2023).
2. Comparison between the simulations results and the satellite retrievals. For this comparison, since the domain covered by the satellite retrieval data set differs from that of the ash dispersion simulations in terms of both extent (which, in turn, changes over time) and spatial resolution and the time of the retrievals do not necessarily coincide with the output times of the simulations, we had to:
   a. Identify the satellite retrievals times which showed an ash cloud in the computational domain.
   b. Select the simulated output time step that is the closest to the satellite retrieval time validity.
   c. Re-map the satellite retrieved-ML (ML_{sat}) onto the computational domain grid. To do so, for each computational domain cell we averaged all the ML_{sat} that are located in the cell and assigned the resulting average to the whole computational domain cell;

With this procedure we finally obtained time series of domain-averaged observed and simulated ML ($\overline{ML_{sat}}$ and $\overline{ML_{sim}}$, respectively) and of the Root Mean Squared Error (RMSE) between ML_{sat} and ML_{sim} over all the N cells in which the deviation $ML_{sat} - ML_{sim} > 1E^{-10}$ g m^{-2}, calculated as:

$$\text{RMSE} = \sqrt{\frac{\sum_{i=1}^{N} \left(ML_{sat,i} - ML_{,i}\right)^2}{N}} \tag{10}$$

In the following section we review the results of these analyses.

4. Results

Figure 3 shows the results of the ash dispersion simulations for the two tests described above, specifically, the complete time series of the extent of the area covered by the ash cloud defined as the area of the domain where ML > 0.5 g m^{-2}. In particular, Figure 3a displays the time series of the difference ($\Delta A\%$) between the areas obtained with the original and modified ESPs time series for the two tests. In both cases, there is always a negative difference between the two areas, meaning that a decrease of the area affected by the ash cloud always occurs when applying the corrections presented in Section 2.2. However, test_DBM correction almost always results in a significantly higher decrease of the ash cloud extent, as it is evident by looking at the plots shown in Figure 3. A common feature between the two tests is that the time evolution of A and of $\Delta A\%$ is not steady, with phases that clearly show a much lower (and almost negligible in the test_WM) decrease in the ash cloud extent. This occurs when the plume was not bent over, as it can be inferred by comparing Figure 3 with the time series of h and H_c shown in Figure 1b. In particular, with WM when there is no top plume height correction the simulation results coincide, since only the top plume height is affected in test_WM; instead, in test_DBM the wind entrainment

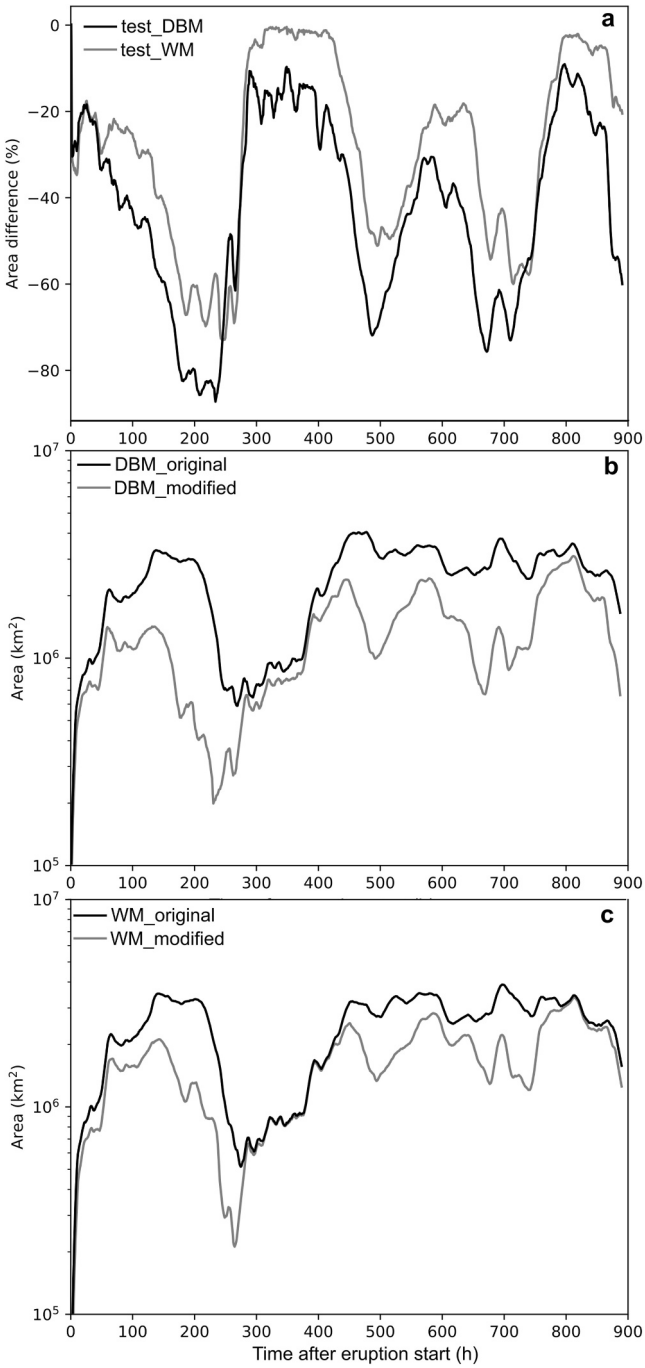

Figure 3. (a) Difference (%) of the area of the ash cloud where $ML_{sim} > 0.5$ g m^{-2} between the two simulations (original and modified eruption source parameters) for the two tests (test_DBM and test_WM). (b) Time series of the area of the ash cloud where $ML_{sim} > 0.5$ g m^{-2} for the DBM_original (black line) and DBM_modified simulation (gray line) for the test_DBM. (c) Time series of the area of the ash cloud where $ML_{sim} > 0.5$ g m^{-2} for the WM_original (black line) and WM_modified simulation (gray line) for the test 2.

coefficient β was also changed, hence, a difference, though reduced compared to the rest of the time series, can still be seen between the two simulations in test_DBM.

Figure 4 shows the time series of the volume of the domain V in which the ash mass concentration C is above two of the critical concentration thresholds indicated by ICAO, namely, 2 mg m^{-3} (medium concentration) and 10 mg m^{-3} (very high concentration). The calculation was conducted for both the tests. As for the ash ML, in both tests the extent of the ash cloud, in this case quantified via V, significantly decreases when applying the corrections in the two tests and the decreases is more evident in test_DBM when applying the corrections to DBM, as expected and in agreement with what was observed on the area A (Figure 3).

We then compared ML_{sim} with ML_{sat} from the MODIS instruments aboard the polar AQUA and TERRA satellites and processed with the LUT_p and VPR procedures. For the time stamps of the satellite retrievals that satisfied the conditions explained in Section 3, we extracted the ML_{sim} for the two simulations (original and modified ESPs time series) of the two tests. Figure 5 shows example maps of the simulated mass loadings for the two tests, specifically: DBM_original and DBM_modified for test_DBM (Figures 5a and 5b); WM_original and WM_modified for test_WM (Figures 5c and 5d). Furthermore, it shows the observed mass loadings obtained with MODIS-AQUA with the LUT_p algorithm (Figure 5e) and with True Color Corrected Reflectances (Figure 5f) on the 10 May 2010 at 13.15 UTC; the simulated outputs refer to the time step on the 15 May 2010 at 13.00 UTC.

The reduction of the extent of the cloud is evident in Figure 5 for both test_DBM and test_WM, particularly in the former with DBM. However, the satellite retrieved ash cloud, as tracked by the ML contour, is less extended although with comparable peak values. Upon looking at the MODIS AQUA True Color Corrected Reflectances in Figure 5f, which highlights the cloud cover, it can be inferred how part of the ash cloud was impacted by the clouds, which partly explains the underestimation of the observed ML compared to the modeled ML.

Table S1 in Supporting Information S1 lists all the time stamps selected from the AQUA and TERRA retrievals (with the LUT algorithm) for the comparisons with the simulated outputs, based on the criteria explained in the previous section. Figure 6 shows the simulated and observed (with the LUT algorithm) ML (averaged over the whole ash cloud area) for all the considered time steps, together with the RMSE calculated using Equation 10. Results with the VPR algorithm are almost identical (see Table 3) and therefore are shown in the Figure S1 in Supporting Information S1, together with the related time stamps in Table S2 in Supporting Information S1. Figures 6a and 6b display the ML_{sim} obtained in the first test (with DBM) and the satellite-retrieved ML_{sat} observed by AQUA and TERRA, respectively. In both cases, the satellite-retrieved ML_{sat}, also shown with the related uncertainty, are significantly lower than the simulated ones; however, ML_{sim} significantly decreases when applying the ESPs correction, in some time steps almost matching the observed ML_{sat}. Similar considerations can be done for Test_WM (Figures 6c and 6d), but with some time steps in which no improvement can be observed in the WM_modified simulation; these time steps are those in which the plume was not bent over and no top plume height correction was applied and hence the two ML_{sim} lines (WM_original and WM_modified) almost coincide (e.g., around the fifth time stamp in Figures 6c and 6d), as already discussed for Figure 3. The improvement of the

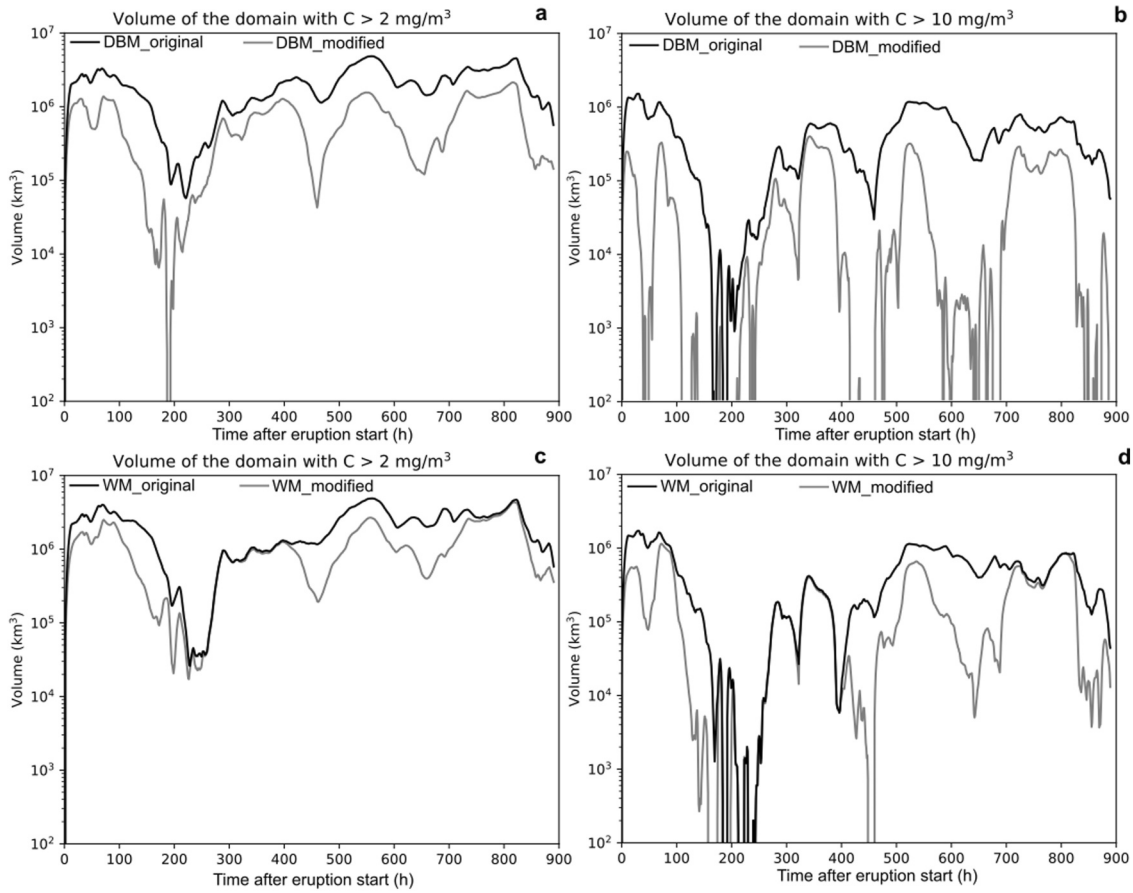

Figure 4. (a) Volume of the computational domain with ash mass concentration larger than 2 mg m^{-3} for the DBM_original (black line) and the DBM_modified simulation (gray line) for the first test (test_DBM). (b) Volume of the computational domain with ash mass concentration larger than 10 mg m^{-3} for the DBM_original (black line) and the DBM_modified simulation (gray line) for the first test (test_DBM). (c) Volume of the computational domain with ash mass concentration larger than 2 mg m^{-3} for the WM_original (black line) and the WM_modified simulation (gray line) for the second test (test_WM). (d) Volume of the computational domain with ash mass concentration larger than 10 mg m^{-3} for the WM_original (black line) and the WM_modified simulation (gray line) for the second test (test_WM).

simulations with the proposed corrections is further highlighted by the RMSE time series (Figures 6e and 6f), which show a significant decrease for the modified ESPs simulations, with the exception of the Test_WM in the time steps in which no top plume height correction was applied. The time-averaged RMSE for the simulations of the two tests and the two considered satellite are listed in detail in Table 3 and further corroborates the decrease of the error when applying the corrections. Furthermore, they show a slightly higher RMSE when comparing with TERRA retrievals; this can be explained by the almost systematic lower ML_{sat} observed with TERRA, as can be seen by looking at Figures 6a–6d.

5. Conclusions

In this study we showed that, by applying the corrections that are listed in Table 2 and were originally proposed by Dürig et al. (2023b) to improve the performance of DBM and WM models in the calculation of MER during the Eyja2010 eruption, we significantly improved the capability of FALL3D to reproduce satellite-retrieved observed ML. This stresses the importance of applying top plume height corrections and, if possible, fine tuning the wind entrainment coefficients when using wind affected plume models in order to initialize ash dispersal simulations.

Despite the improvements, the simulated ML were almost constantly higher than the satellite-retrieved ones. This can be attributed to both the modeling and the satellite retrieval limitations. The former include uncertainty in the top plume height. In fact, as already discussed in Dioguardi et al. (2020), the top plume height time series obtained by the C-band radar installed in Keflavík was affected by an uncertainty of ±1.2 km. In this study, we just considered the best estimate of the top plume height. As already shown in Dioguardi

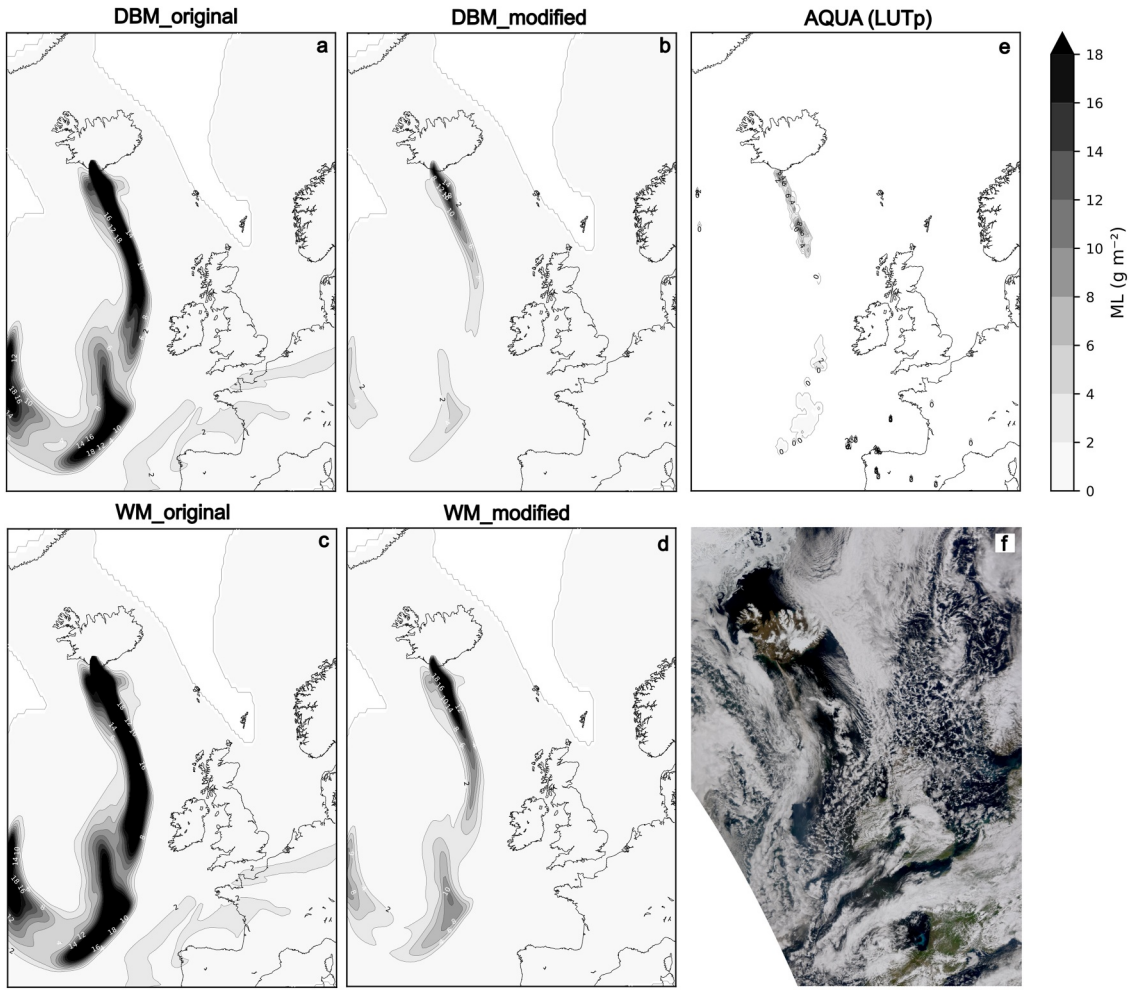

Figure 5. Simulated ML on the 10 May 2010 at 13:00 UTC for: (a) DBM_original, (b) DBM_modified, (c) WM_original, (d) WM_modifiedt, and (e) Satellite retrieved (MODIS-AQUA with LUT$_p$ algorithm) ML on the 10 May 2010 at 13.15 UTC. (f) True Color image from MODIS/AQUA (10 May 2010) taken from https://ladsweb.modaps.eosdis.nasa.gov/view-data/ and processed using the Pytroll/Satpy software (Raspaud et al., 2023).

et al. (2020), by considering the minimum estimate the MER would be decreased by almost 80% on average for wind-affected models like DBM and WM, hence cascading in a reduction of the simulated averaged ML. The minimum estimate would be much closer to the satellite retrieved outputs. Satellite retrieval limitations include "visibility" of the ash particles in terms of size and altitude. Recently, Saint et al. (2024) stated that satellite can better detect particles smaller than 16 μm, whilst in our study we considered all particles up to 20 μm. The fraction between 16 and 20 μm accounts for about 2.2% of the weight fractions of the TGSD of Bonadonna et al. (2011), which is used in this study. Therefore, according to the findings of Saint et al. (2024), we would slightly overestimate the ML and the area affected by ash since the MER at the source would be reduced by 2.2%. Furthermore, Saint et al. (2024) also found that satellites do not detect particles below 3 km a.s.l., whilst we calculated the ML by integrating the simulated concentrations from the sea level to the top of the ash cloud; this would further explain the overestimation of the simulated ML over the satellite retrieved-ones. Additionally, the effect of the cloud cover should be taken into account when comparing simulated versus satellite-retrieved ML. As shown in Figure 5, clouds obliterated the ash cloud in several portions, hence artificially enhancing the difference between simulated and observed ML, even after the MER corrections here presented. For example, Saint et al. (2024) showed that ML would be underestimated for ash columns with column loadings $>\sim 7$ g m^{-2} in the presence of clouds. Finally, it is to note that the simulations in our study were carried out assuming a uniform release of ash from the volcanic vent to the top plume height for simplicity and focusing solely on the parameters being investigated in this study.

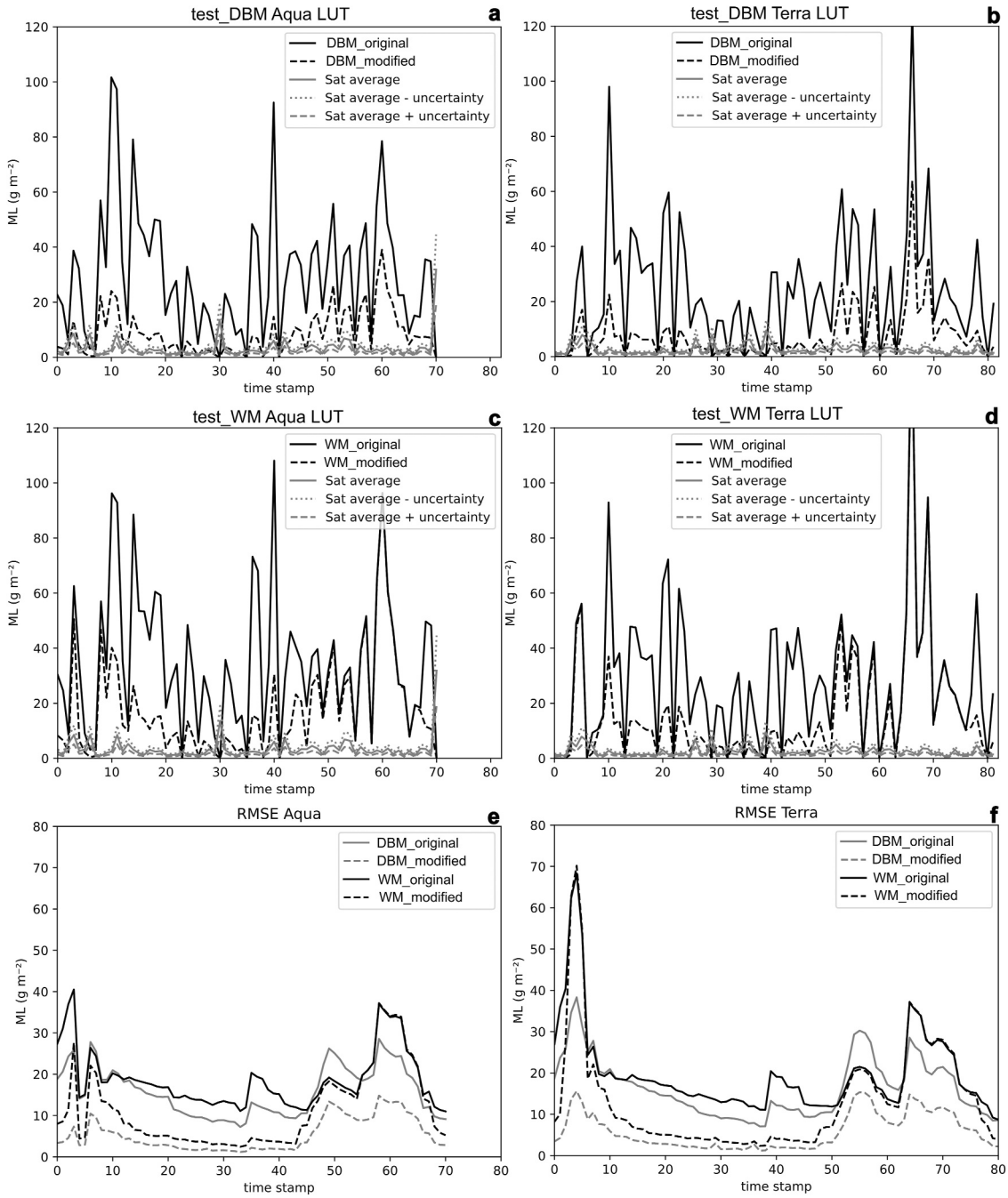

Figure 6. (a) Simulated versus AQUA satellite retrieved-ML (LUT algorithm) for the test_DBM. Time on the *x* axis represents the time stamps' numbering in Table S1 in Supporting Information S1. Black solid line: DBM_original; Black dashed line: DBM_modified; Gray solid line: satellite retrieval; Gray dashed line: satellite retrieval minus the uncertainty; and Gray dotted line: satellite retrieval plus the uncertainty. (b) Simulated versus TERRA satellite retrieved-ML (LUT algorithm) for the test_DBM. Black solid line: DBM_original; Black dashed line: DBM_modified; Gray solid line: satellite retrieval; Gray dashed line: satellite retrieval minus the uncertainty; and Gray dotted line: satellite retrieval plus the uncertainty. (c) Simulated versus AQUA satellite retrieved-ML (LUT algorithm) for the test_WM model. Black solid line: WM_original; Black dashed line: WM_modified; Gray solid line: satellite retrieval; Gray dashed line: satellite retrieval minus the uncertainty; and Gray dotted line: satellite retrieval plus the uncertainty. (d) Simulated versus TERRA satellite retrieved-ML (LUT algorithm) for the test_WM. Black solid line: WM_original; Black dashed line: WM_modified; Gray solid line: satellite retrieval; Gray dashed line: satellite retrieval minus the uncertainty; and Gray dotted line: satellite retrieval plus the uncertainty. (e) Root Mean Squared Error (RMSE) between simulated and AQUA satellite retrieved-ML. Gray solid line: DB_original; Gray dashed line: DB_modified; Black solid line: WM_original; and Black dashed line: WM_modified. (f) RMSE between simulated and TERRA satellite retrieved-ML. Gray solid line: DB_original; Gray dashed line: DB_modified; Black solid line: WM_original; and Black dashed line: WM_modified.

Table 3
Domain-Averaged Root Mean Squared Error for the Two Tests and for Each Satellite Retrieval

Simulation ID	Aqua—LUT	Aqua—VPR	Terra—LUT	Terra—VPR
DBM_original	15.88	15.90	16.33	15.95
DBM_modified	5.41	5.35	5.80	5.57
WM_original	18.71	18.76	19.61	19.06
WM_modified	11.23	11.26	13.07	12.40

One needs to consider, though, that volcanic ash can be released from different non-uniform vertical profiles, which can significantly affect the simulated ML (e.g., Harvey et al., 2025). Finally, other processes may affect the ash particles residence time in the atmosphere, hence the prediction capabilities of the numerical models used to simulate ash dispersion, like ash particles interactions with aerosols particles that increase their size and favor sedimentation (Muser et al., 2020).

The results presented here further raises awareness of the need to improve simplified plume models used to initialize ash dispersal simulations for operational applications like civil aviation safety. If the improvements taken into account in this study are obtained using an a-posteriori analysis, they could be included in procedures for real time applications, for example, during eruptive crises. For example, whilst the top plume height correction is very challenging to measure in real time, the Devenish (2016) formula performed well and this can be used in conjunction with the estimation of the wind entrainment coefficient, which remains the only unknown in real-time applications and, as such, it can be treated as an unknown varying parameter in ensemble simulations.

Conflict of Interest

The authors declare no conflicts of interest relevant to this study.

Data Availability Statement

Hersbach et al. (2018a, 2018b) was downloaded from the Copernicus Climate Change Service (2023a, 2023b).

The results contain modified Copernicus Climate Change Service information 2020. Neither the European Commission nor ECMWF is responsible for any use that may be made of the Copernicus information or data it contains.

Terra/MODIS and Aqua/MODIS Level 1B Calibrated Radiances at 1 km were acquired from the Level-1 and Atmosphere Archive & Distribution System (LAADS) Distributed Active Archive Center (DAAC), located in the Goddard Space Flight Center in Greenbelt, Maryland (https://ladsweb.nascom.nasa.gov/).

All the other data and instructions necessary to replicate the simulations and data analysis presented in this study are available at https://doi.org/10.5281/zenodo.17287724 (Dioguardi, 2025a).

The Python codes used to analyze the data and produce the outputs presented in this manuscript are available at https://doi.org/10.5281/zenodo.17383932 (Dioguardi, 2025b).

Acknowledgments
FD carried out this study within the RETURN Extended Partnership and received funding from the European Union Next-Generation EU (National Recovery and Resilience Plan – NRRP, Mission 4, Component 2, Investment 1.3 – D.D. 1243 2/8/2022, PE0000005). SC, LG, LM, and DS were supported by the: (a) VOlcanic pLume chAracterization using sounding balloOns (VOLANDO) project funded by European Union—Next Generation EU, Mission 4 Component 1 CUP 1207.10.00. (b) GET-IT project funded by ESA, Contract 4000146211/24/I-KE. The computational work has been executed on the IT resources of the ReCaS-Bari data center, which have been made available by the following projects financed by the MIUR (Italian Ministry for Education, University and Research): ReCaS (Azione I - Interventi di rafforzamento strutturale, PONa3_00052, Avviso 254/Ric) and PRISMA (Asse II - Sostegno all'innovazione, PON04a2_A), within the "PON Ricerca e Competitività 2007-2013" program, and DHTCS (now IPCEI-HPCBDA, Avviso D. D. n. 424 del 28.02.2018), IBiSCo (PIR01_00011), CNRBiOmics (PIR01_00017) and LifeWatchPLUS (PIR-01_00028) within the "PON Ricerca e Innovazione 2014-2020" program Azione II.1, CUP I66C18000100006, ICSC and TeRABIT within the "PNRR – Avviso n 3264 per il "Rafforzamento e creazione di Infrastrutture di Ricerca", Missione 4, "Istruzione e Ricerca"". We thank Marie Hagenbourger and an anonymous reviewer for their feedbacks and constructive remarks that helped improving our manuscript. We also thank Susan Loughlin (British Geological Survey) for her fruitful comments and suggestions. This work is published with permission of the Executive Director of British Geological Survey (UKRI).

References

Arason, P., Petersen, G. N., & Bjornsson, H. (2011). Observations of the altitude of the volcanic plume during the eruption of Eyjafjallajökull, April–May 2010. *Earth System Science Data*, *3*(1), 9–17. https://doi.org/10.5194/essd-3-9-2011

Aubry, T. J., Engwell, S., Bonadonna, C., Carazzo, G., Scollo, S., Van Eaton, A. R., et al. (2021). The independent volcanic eruption source parameter archive (IVESPA, version 1.0): A new observational database to support explosive eruptive column model validation and development. *Journal of Volcanology and Geothermal Research*, *417*, 107295. https://doi.org/10.1016/j.jvolgeores.2021.107295

Aubry, T. J., Engwell, S., Bonadonna, C., Mastin, L. G., Carazzo, G., Van Eaton, A. R., et al. (2023). New insights into the relationship between mass eruption rate and volcanic column height based on the IVESPA dataset. *Geophysical Research Letters*, *50*(14), e2022GL102633. https://doi.org/10.1029/2022GL102633

Beckett, F. M., Barsotti, S., Burton, R., Dioguardi, F., Engwell, S., Hort, M., et al. (2024). Conducting volcanic ash cloud exercises: Practising forecast evaluation procedures and the pull-through of scientific advice to the London VAAC. *Bulletin of Volcanology*, *86*(7), 63. https://doi.org/10.1007/s00445-024-01717-9

Beckett, F. M., Witham, C. S., Leadbetter, S. J., Crocker, R., Webster, H. N., Hort, M. C., et al. (2020). Atmospheric dispersion modelling at the London VAAC: A review of developments since the 2010 Eyjafjallajökull volcano ash cloud. *Atmosphere*, *11*(4), 352. https://doi.org/10.3390/atmos11040352

Birnbaum, J., Lev, E., Hernandez, P. A., Barrancos, J., Padilla, G. D., Asensio-Ramos, M., et al. (2023). Temporal variability of explosive activity at Tajogaite volcano, Cumbre Vieja (Canary Islands), 2021 eruption from ground-based infrared photography and videography. *Frontiers in Earth Science*, *11*, 1193436. https://doi.org/10.3389/feart.2023.1193436

Bonadonna, C., Genco, R., Gouhier, M., Pistolesi, M., Cioni, R., Alfano, F., et al. (2011). Tephra sedimentation during the 2010 Eyjafjallajökull eruption (Iceland) from deposit, radar, and satellite observations. *Journal of Geophysical Research*, *116*(B12), B12202. https://doi.org/10.1029/2011JB008462

Bonadonna, C., Pistolesi, M., Cioni, R., Degruyter, W., Elissondo, M., & Baumann, V. (2015). Dynamics of wind-affected volcanic plumes: The example of the 2011 Cordón Caulle eruption, Chile. *Journal of Geophysical Research Solid Earth*, *120*(4), 2242–2261. https://doi.org/10.1002/2014JB011478

Bruckert, J., Hoshyaripour, G. A., Horváth, Á., Muser, L. O., Prata, F. J., Hoose, C., & Vogel, B. (2022). Online treatment of eruption dynamics improves the volcanic ash and SO_2 dispersion forecast: Case of the 2019 Raikoke eruption. *Atmospheric Chemistry and Physics*, *22*(5), 3535–3552. https://doi.org/10.5194/acp-22-3535-2022

Bursik, M. (2001). Effect of wind on the rise height of volcanic plumes. *Geophysical Research Letters*, *28*(18), 3621–3624. https://doi.org/10.1029/2001GL013393

Büttner, R., Zimanowski, B., & Röder, H. (2000). Short-time electrical effects during volcanic eruption: Experiments and field measurements. *Journal of Geophysical Research*, *105*(B2), 2819–2827. https://doi.org/10.1029/1999JB900370

Byun, D., & Schere, K. (2006). Review of the governing equations, computational algorithms, and other components of the Models-3 community multiscale air quality (CMAQ) modeling system. *Applied Mechanics Reviews*, *59*(2), 51–77. https://doi.org/10.1115/1.2128636

Calvari, S., Büttner, R., Cristaldi, A., Dellino, P., Giudicepietro, F., Orazi, M., et al. (2012). The 7 September 2008 Vulcanian explosion at Stromboli volcano: Multiparametric characterization of the event and quantification of the ejecta. *Journal of Geophysical Research*, *117*, B05201. https://doi.org/10.1029/2011JB009048

Cerminara, M., Esposti Ongaro, T., & Berselli, L. C. (2016). ASHEE-1.0: A compressible, equilibrium–Eulerian model for volcanic ash plumes. *Geoscientific Model Development*, *9*(2), 697–730. https://doi.org/10.5194/gmd-9-697-2016

Cerminara, M., Esposti Ongaro, T., Valade, S., & Harris, A. J. L. (2015). Volcanic plume vent conditions retrieved from infrared images: A forward and inverse modeling approach. *Journal of Volcanology and Geothermal Research*, *300*, 129–147. https://doi.org/10.1016/j.jvolgeores.2014.12.015

Copernicus Climate Change Service. (2023a). Copernicus climate change service: ERA5 hourly data on pressure levels from 1940 to present. *Copernicus Climate Change Service (C3S) Climate Data Store (CDS)*. https://doi.org/10.24381/cds.adbb2d47

Copernicus Climate Change Service. (2023b). Copernicus climate change service: ERA5 hourly data on single levels from 1940 to present. *Copernicus Climate Change Service (C3S) Climate Data Store (CDS)*. https://doi.org/10.24381/cds.adbb2d47

Corradini, S., Guerrieri, L., Brenot, H., Clarisse, L., Merucci, L., Pardini, F., et al. (2021). Tropospheric volcanic SO_2 mass and flux retrievals from satellite. The Etna December 2018 eruption. *Remote Sensing*, *13*(11), 2225. https://doi.org/10.3390/rs13112225

Corradini, S., Guerrieri, L., Lombardo, V., Merucci, L., Musacchio, M., Prestifilippo, M., et al. (2018). Proximal monitoring of the 2011-2015 Etna lava fountains using MSG-SEVIRI data. *Geosciences, Special Issue on Volcanic Plumes: Impacts on the Atmosphere and Insights into Volcanic Processes*, *8*(4), 140. https://doi.org/10.3390/geosciences8040140

Corradini, S., Merucci, L., & Arnau, F. (2011). Volcanic ash cloud properties: Comparison between MODIS satellite retrievals and FALL3D transport model. *IEEE Geoscience and Remote Sensing Letters*, *8*(2), 248–252. https://doi.org/10.1109/LGRS.2010.2064156

Corradini, S., Merucci, L., Prata, A. J., & Piscini, A. (2010). Volcanic ash and SO_2 in the 2008 Kasatochi eruption: Retrievals comparison from different IR satellite sensors. *Journal of Geophysical Research*, *115*(D2), D00L21. https://doi.org/10.1029/2009JD013634

Corradini, S., Montopoli, M., Guerrieri, L., Ricci, M., Scollo, S., Merucci, L., et al. (2016). A multi-sensor approach for the volcanic ash cloud retrievals and eruption characterization. *Remote Sensing, Special Issue on Volcano Remote Sensing*, *8*(1), 58. https://doi.org/10.3390/rs8010058

Corradini, S., Pugnaghi, S., Piscini, A., Guerrieri, L., Merucci, L., Picchiani, M., & Chini, M. (2014). Volcanic ash and SO_2 retrievals using synthetic MODIS TIR data: Comparison between inversion procedures and sensitivity analysis. *Annals of Geophysics, Special Issue on "Atmospheric Emissions from Volcanoes"*, *57*, 4. https://doi.org/10.4401/ag-6616

Corradini, S., Spinetti, C., Carboni, E., Tirelli, C., Buongiorno, M. F., Pugnaghi, S., & Gangale, G. (2008). Mt. Etna tropospheric ash retrieval and sensitivity analysis using moderate resolution imaging spectroradiometer measurements. *Journal of Applied Remote Sensing*, *2*(1), 023550. https://doi.org/10.1117/1.3046674

Costa, A., Macedonio, G., & Folch, A. (2006). A three-dimensional Eulerian model for transport and deposition of volcanic ashes. *Earth and Planetary Science Letters*, *241*(3–4), 634–647. https://doi.org/10.1016/j.epsl.2005.11.019

Degruyter, W., & Bonadonna, C. (2012). Improving on mass flow rate estimates of volcanic eruptions. *Geophysical Research Letters*, *39*(16), 1–6. https://doi.org/10.1029/2012GL052566

Dellino, P., Gudmundsson, M. T., Larsen, G., Mele, D., Stevenson, J. A., Thordarson, T., & Zimanowski, B. (2012). Ash from the Eyjafjallajökull eruption (Iceland): Fragmentation processes and aerodynamic behavior. *Journal of Geophysical Research*, *117*, B00C04. https://doi.org/10.1029/2011JB008726

de Michele, M., Raucoules, D., Corradini, S., Merucci, L., Salerno, G., Sellitto, P., & Carboni, E. (2019). Volcanic cloud top height estimation using the plume elevation model procedure applied to orthorectified landsat 8 data. Test case: 26 October 2013 Mt. Etna eruption. *Remote Sensing*, *11*(7), 785. https://doi.org/10.3390/rs11070785

de'Michieli Vitturi, M., Neri, A., & Barsotti, S. (2015). PLUME-MoM 1.0: A new integral model of volcanic plumes based on the method of moments. *Geoscientific Model Development*, *8*(8), 2447–2463. https://doi.org/10.5194/gmd-8-2447-2015

Devenish, B. J. (2013). Using simple plume models to refine the source mass flux of volcanic eruptions according to atmospheric conditions. *Journal of Volcanology and Geothermal Research*, *256*, 118–127. https://doi.org/10.1016/j.jvolgeores.2013.02.015

Devenish, B. J. (2016). Estimating the total mass emitted by the eruption of Eyjafjallajökull in 2010 using plume-rise models. *Journal of Volcanology and Geothermal Research*, *326*, 114–119. https://doi.org/10.1016/j.jvolgeores.2016.01.005

Dioguardi, F. (2025a). Data and list of commands required to run and post-process results of the Eyjafjallajökull 2010 FALL3D simulations [Dataset]. *Zenodo*. https://doi.org/10.5281/zenodo.17287724

Dioguardi, F. (2025b). *FabioDioguardi/ashml_analysis: v1.0 (v1.0)*. Zenodo. https://doi.org/10.5281/zenodo.17383932

Dioguardi, F., Beckett, F., Dürig, T., & Stevenson, J. A. (2020). The impact of eruption source parameter uncertainties on ash dispersion forecasts during explosive volcanic eruptions. *Journal of Geophysical Research: Atmospheres*, *125*(17), e2020JD032717. https://doi.org/10.1029/2020JD032717

Dioguardi, F., Dellino, P., & Mele, D. (2018). A new one-equation model of fluid drag for irregularly shaped particles valid over a wide range of Reynolds number. *Journal of Geophysical Research Solid Earth*, *123*(1), 144–156. https://doi.org/10.1002/2017JB014926

Durant, A. J., Bonadonna, C., & Horwell, C. J. (2010). Atmospheric and environmental impacts of volcanic particulates. *Elements*, *6*(4), 235–240. https://doi.org/10.2113/gselements.6.4.235

Dürig, T., Gudmundsson, M. T., & Dellino, P. (2015a). Reconstruction of the geometry of volcanic vents by trajectory tracking of fast ejecta - The case of the Eyjafjallajökull 2010 eruption (Iceland). *Earth Planets and Space*, *67*(1), 64. https://doi.org/10.1186/s40623-015-0243-x

Dürig, T., Gudmundsson, M. T., Dioguardi, F., & Schmidt, L. S. (2023b). Quantifying the effect of wind on volcanic plumes: Implications for plume modeling. *Journal of Geophysical Research: Atmospheres*, *128*(2), e2022JD037781. https://doi.org/10.1029/2022JD037781

Dürig, T., Gudmundsson, M. T., Dioguardi, F., Woodhouse, M., Björnsson, H., Barsotti, S., et al. (2018). REFIR- A multi-parameter system for near real-time estimates of plume-height and mass eruption rate during explosive eruptions. *Journal of Volcanology and Geothermal Research*, *360*, 61–83. https://doi.org/10.1016/j.jvolgeores.2018.07.003

Dürig, T., Gudmundsson, M. T., Karmann, S., Zimanowski, B., Dellino, P., Rietze, M., & Büttner, R. (2015b). Mass eruption rates in pulsating eruptions estimated from video analysis of the gas thrust-buoyancy transition—A case study of the 2010 eruption of Eyjafjallajökull, Iceland. *Earth Planets and Space*, *67*(1), 180. https://doi.org/10.1186/s40623-015-0351-7

Dürig, T., Schmidt, L. S., & Dioguardi, F. (2023a). Optimizing mass eruption rate estimates by combining simple plume models. *Frontiers in Earth Science*, *11*, 1250686. https://doi.org/10.3389/feart.2023.1250686

Esposti Ongaro, T., Cavazzoni, C., Erbacci, G., Neri, A., & Salvetti, M. V. (2007). A parallel multiphase flow code for the 3D simulation of explosive volcanic eruptions. *Parallel Computing*, *33*(7–8), 541–560. https://doi.org/10.1016/j.parco.2007.04.003

Folch, A., Costa, A., & Basart, S. (2012). Validation of the FALL3D ash dispersion model using observations of the 2010 Eyjafjallajökull volcanic ash clouds. *Atmospheric Environment*, *48*, 165–183. https://doi.org/10.1016/j.atmosenv.2011.06.072

Folch, A., Costa, A., & Macedonio, G. (2016). FPLUME-1.0: An integral volcanic plume model accounting for ash aggregation. *Geoscientific Model Development*, *9*(1), 431–450. https://doi.org/10.5194/gmd-9-431-2016

Folch, A., Mingari, L., Gutierrez, N., Hanzich, M., Macedonio, G., & Costa, A. (2020). FALL3D-8.0: A computational model for atmospheric transport and deposition of particles, aerosols and radionuclides – Part 1: Model physics and numerics. *Geoscientific Model Development*, *13*(3), 1431–1458. https://doi.org/10.5194/gmd-13-1431-2020

Freret-Lorgeril, V., Bonadonna, C., Corradini, S., Donnadieu, F., Guerrieri, L., Lacanna, G., et al. (2021). Examples of multi-sensor determination of eruptive source parameters of explosive events at Mount Etna. *Remote Sensing*, *13*(11), 2097. https://doi.org/10.3390/rs13112097

Freret-Lorgeril, V., Bonadonna, C., Corradini, S., Guerrieri, L., Lemus, J., Donnadieu, F., et al. (2021). Tephra characterization and multi-disciplinary determination of eruptive source parameters of a weak paroxysm at Mount Etna (Italy). *Journal of Volcanology and Geothermal Research*, *421*, 107431. https://doi.org/10.1016/j.jvolgeores.2021

Giehl, C., Brooker, R. A., Marxer, H., & Nowak, M. (2017). An experimental simulation of volcanic ash deposition in gas turbines and implications for jet engine safety. *Chemical Geology*, *461*, 160–170. https://doi.org/10.1016/j.chemgeo.2016.11.024

Grindle, T. J., & Burcham, F. W. (2002). Even minor volcanic ash encounters can cause major damage to aircraft. *ICAO Journal*, *57*, 12–14.

Gudmundsson, M. T., Thordarson, T., Hoskuldsson, A., Larsen, G., Bjornsson, H., Prata, F. J., et al. (2012). Ash generation and distribution from the April-May 2010 eruption of Eyjafjallajökull, Iceland. *Scientific Reports*, *2*, 1–12. https://doi.org/10.1038/srep00572

Guerrieri, L., Corradini, S., Merucci, L., Stelitano, D., Prata, F., Lambertucci, L., et al. (2025). A novel simplified ground-based TIR system for volcanic plume geometry, SO_2 columnar abundance, and flux retrievals. *Atmospheric Measurement Techniques*, *18*(19), 5281–5297. https://doi.org/10.5194/amt-18-5281-2025

Guerrieri, L., Corradini, S., Theys, N., Stelitano, D., & Merucci, L. (2023). Volcanic clouds characterization of the 2020–2022 sequence of Mt. Etna lava fountains using MSG-SEVIRI and products' cross-comparison. *Remote Sensing*, *15*(8), 2055. https://doi.org/10.3390/rs15082055

Guerrieri, L., Merucci, L., Corradini, S., & Pugnaghi, S. (2015). Evolution of the 2011 Mt. Etna ash and SO_2 lava fountain episodes using SEVIRI data and VPR retrieval approach. *Journal of Volcanology and Geothermal Research*, *291*, 63–71. https://doi.org/10.1016/j.jvolgeores.2014.12.016

Harris, A. J. L. (2013). *Thermal remote sensing of active volcanoes: A user's manual*. Cambridge University Press.

Harris, A. J. L., Delle Donne, D., Dehn, J., Ripepe, M., & Worden, A. K. (2013). Volcanic plume and bomb field masses from thermal infrared camera imagery. *Earth and Planetary Science Letters*, *365*, 77–85. https://doi.org/10.1016/j.epsl.2013.01.004

Harris, A. J. L., Gurioli, L., Hughes, E. E., & Lagreulet, S. (2012). Impact of the Eyjafjallajökull ash cloud: A newspaper perspective. *Journal of Geophysical Research*, *117*(B9), B00C08. https://doi.org/10.1029/2011JB008735

Harvey, N. J., Herzog, M., Dacre, H. F., & Webster, H. N. (2025). A comparison of volcanic ash source term characteristics estimated by source inversion and plume rise modelling methods: Raikoke 2019. *Journal of Volcanology and Geothermal Research*, *462*, 108304. https://doi.org/10.1016/j.jvolgeores.2025.108304

Hersbach, H., Bell, B., Berrisford, P., Biavati, G., Horányi, A., Muñoz Sabater, J., et al. (2018a). ERA5 hourly data on pressure levels from 1940 to present [Dataset]. *Copernicus Climate Change Service (C3S) Climate Data Store (CDS)*. https://doi.org/10.24381/cds.bd0915c6

Hersbach, H., Bell, B., Berrisford, P., Biavati, G., Horányi, A., Muñoz Sabater, J., et al. (2018b). ERA5 hourly data on single levels from 1940 to present [Dataset]. *Copernicus Climate Change Service (C3S) Climate Data Store (CDS)*. https://doi.org/10.24381/cds.adbb2d47

Hochfeld, I., Hort, M., Schwalbe, E., & Dürig, T. (2022). Eruption dynamics of Anak Krakatau volcano (Indonesia) estimated using photogrammetric methods. *Bulletin of Volcanology*, *84*(8), 73. https://doi.org/10.1007/s00445-022-01579-z

International Civil Aviation Organization. (2023). MIDANPIRG meteorology sub-group eleventh meeting (MET SG/11), Cairo, Egypt, 14–15 November 2023. Retrieved from https://www.icao.int/MID/Documents/2023/MET%20SG11/WP%2010.pdf

Johnson, J. B., & Ripepe, M. (2011). Volcano infrasound: A review. *Journal of Volcanology and Geothermal Research*, *206*(3–4), 61–69. https://doi.org/10.1016/j.jvolgeores.2011.06.006

Jones, A. R., Thomson, D. J., Hort, M. C., & Devenish, B. (2007). The U.K. Met Office's next-generation atmospheric dispersion model, NAME III. In C. Borrego & A. L. Norman (Eds.), *Air pollution modelling and its application XVII (Proceedings of the 27th NATO/CCMS international technical meeting on air pollution modelling and its application)* (pp. 589). Springer.

Jonsson, J. (1988). *Geological map of eyjafjöll*. Hveragerði: Research Institute Neðri As Hveragerði.

Kienle, J., Kyle, P. R., Self, S., Motyka, R. J., & Lorenz, V. (1980). Ukinrek Maars, Alaska, I. April 1977 eruption sequence, petrology and tectonic setting. *Journal of Volcanology and Geothermal Research*, *7*(1–2), 11–37. https://doi.org/10.1016/0377-0273(80)90018-9

Marti, A., Folch, A., Jorba, O., & Janjic, Z. (2017). Volcanic ash modeling with the online NMMB-MONARCH-ASH v1.0 model: Model description, case simulation, and evaluation. *Atmospheric Chemistry and Physics*, *17*(6), 4005–4030. https://doi.org/10.5194/acp-17-4005-2017

Marzano, F. S., Mereu, L., Scollo, S., Donnadieu, F., & Bonadonna, C. (2020). Tephra mass eruption rate from ground-based X-Band and L-Band microwave radars during the November 23, 2013, Etna paroxysm. *IEEE Transactions on Geoscience and Remote Sensing*, *58*(5), 3314–3327. https://doi.org/10.1109/TGRS.2019.2953167

Mastin, L. G. (2014). Testing the accuracy of a 1-D volcanic plume model in estimating mass eruption rate. *Journal of Geophysical Research: Atmospheres*, *119*(5), 2474–2495. https://doi.org/10.1002/2013JD020604

Mastin, L. G., Guffanti, M., Servranckx, R., Webley, P., Barsotti, S., Dean, K., et al. (2009). A multidisciplinary effort to assign realistic source parameters to models of volcanic ash-cloud transport and dispersion during eruptions. *Journal of Volcanology and Geothermal Research*, *186*(1–2), 10–21. https://doi.org/10.1016/j.jvolgeores.2009.01.008

Merucci, L., Zakšek, K., Carboni, E., & Corradini, S. (2016). Stereoscopic estimation of volcanic cloud-top height from two geostationary satellites. *Remote Sensing, Special Issue on Volcano Remote Sensing*, *8*(3), 206–2016. https://doi.org/10.3390/rs8030206

Montopoli, M. (2016). Velocity profiles inside volcanic clouds from three-dimensional scanning microwave dual-polarization Doppler radars. *Journal of Geophysical Research: Atmospheres*, *121*(13), 7881–7900. https://doi.org/10.1002/2015JD023464

Muser, L. O., Hoshyaripour, G. A., Bruckert, J., Horváth, Á., Malinina, E., Wallis, S., et al. (2020). Particle aging and aerosol–radiation interaction affect volcanic plume dispersion: Evidence from the Raikoke 2019 eruption. *Atmospheric Chemistry and Physics*, *20*(23), 15015–15036. https://doi.org/10.5194/acp-20-15015-2020

Neale, R., Jadwiga, H. R., Andrew, J. C., Sungsu, P., Peter, H. L., Gettelman, A., et al. (2010). *Description of the NCAR community atmosphere model (CAM 4.0)*. Technical Report NCAR/TN-485+STR. National Center for Atmospheric Research.

Pioli, L., & Harris, A. J. L. (2019). Real-time geophysical monitoring of particle size distribution during volcanic explosions at Stromboli volcano (Italy). *Frontiers in Earth Science*, *7*, 1–13. https://doi.org/10.3389/feart.2019.00052

Prata, A. J. (1989). Observation of volcanic ash clouds using AVHRR-2 radiances. *International Journal of Remote Sensing*, *10*(4–5), 751–761. https://doi.org/10.1080/01431168908903916

Prata, A. J., & Grant, I. F. (2001). Determination of mass loadings and plume heights of volcanic ash clouds from satellite data. In *CSIRO atmospheric research technical paper no. 48*. Commonw. Sci. and Ind. res. Organ.

Pugnaghi, S., Guerrieri, L., Corradini, S., & Merucci, L. (2016). Real time retrieval of volcanic cloud particles and SO_2 by satellite using an improved simplified approach. *Atmospheric Measurement Techniques*, *9*(7), 1–10. https://doi.org/10.5194/amt-9-3053-2016

Pugnaghi, S., Guerrieri, L., Corradini, S., Merucci, L., & Arvani, B. (2013). A new simplified procedure for the simultaneous SO_2 and ash retrieval in a tropospheric volcanic cloud. *Atmospheric Measurement Techniques*, *6*(5), 1315–1327. https://doi.org/10.5194/amt-6-1315-2013

Raspaud, M., Hoese, D., Lahtinen, P., Holl, G., Finkensieper, S., Dybbroe, A., et al. (2023). *pytroll/satpy: Version 0.42.0 (2023/04/28) (v0.42.0)*. Zenodo. https://doi.org/10.5281/zenodo.7875756

Ripepe, M., Bonadonna, C., Folch, A., Delle Donne, D., Lacanna, G., Marchetti, E., & Höskuldsson, A. (2013). Ash-plume dynamics and eruption source parameters by infrasound and thermal imagery: The 2010 Eyjafjallajökull eruption. *Earth and Planetary Science Letters*, *366*, 112–121. https://doi.org/10.1016/j.epsl.2013.02.005

Rizza, U., Brega, E., Caccamo, M. T., Castorina, G., Morichetti, M., Munaò, G., et al. (2020). Analysis of the ETNA 2015 eruption using WRF-chem model and satellite observations. *Atmosphere*, *11*, 1168. https://doi.org/10.3390/atmos11111168

Rizza, U., Donnadieu, F., Morichetti, M., Avolio, E., Castorina, G., Semprebello, A., et al. (2023). Airspace contamination by volcanic ash from sequences of Etna paroxysms: Coupling the WRF-chem dispersion model with near-source L-band radar observations. *Remote Sensing*, *15*, 3760. https://doi.org/10.3390/rs15153760

Saint, C., Beckett, F. M., Dioguardi, F., Kristiansen, N., & Tubbs, R. N. (2024). Using simulated radiances to understand the limitations of satellite-retrieved volcanic ash data and the implications for volcanic ash cloud forecasting. *Journal of Geophysical Research: Atmospheres*, *129*(23), e2024JD041112. https://doi.org/10.1029/2024JD041112

Sæmundsson, K. (1979). Outline of the geology of Iceland. *Jökull Journal*, *29*(1), 7–28. https://doi.org/10.33799/jokull1979.29.007

Scase, M. M., & Hewitt, R. E. (2012). Unsteady turbulent plume models. *Journal of Fluid Mechanics*, *697*, 455–480. https://doi.org/10.1017/jfm.2012.77

Scollo, S., Prestifilippo, M., Bonadonna, C., Cioni, R., Corradini, S., Degruyter, W., et al. (2019). Near-real-time tephra fallout assessment at Mt. Etna, Italy. *Remote Sensing*, *11*(24), 2987. https://doi.org/10.3390/rs11242987

Scollo, S., Prestifilippo, M., Pecora, E., Corradini, S., Merucci, L., Spata, G., & Coltelli, M. (2014). Eruption column height estimation: The 2011-2013 Etna lava fountains. *Annals of Geophysics*, *57*, 2. https://doi.org/10.4401/ag-6396

Sparks, R. S. J., Bursik, M. I., Carey, S. N., Gilbert, J. S., Glaze, L. S., Sigurdsson, H., & Woods, A. W. (1997). *Volcanic plumes*. John Wiley & Sons.

Stein, A. F., Draxler, R. R., Rolph, G. D., Stunder, B. J. B., Cohen, M. D., & Ngan, F. (2015). NOAA's HYSPLIT atmospheric transport and dispersion modeling system. *Bulletin of the American Meteorological Society*, *96*(12), 2059–2077. https://doi.org/10.1175/BAMS-D-14-00110.1

Suzuki, Y. J., & Koyaguchi, T. (2012). 3-D numerical simulations of eruption column collapse: Effects of vent size on pressure-balanced jet/plumes. *Journal of Volcanology and Geothermal Research*, *221–222*, 1–13. https://doi.org/10.1016/j.jvolgeores.2012.01.013

Tournigand, P.-Y., Fernández, J. J. P., Taddeucci, J., Perugini, D., Sesterhenn, J., & Palladino, D. M. (2019). Time evolution of transient volcanic plumes: Insights from fractal analysis. *Journal of Volcanology and Geothermal Research*, *371*, 59–71. https://doi.org/10.1016/j.jvolgeores.2018.12.007

Valade, S. A., Harris, A. J. L., & Cerminara, M. (2014). Plume ascent tracker: Interactive Matlab software for analysis of ascending plumes in image data. *Computer & Geosciences*, *66*, 132–144. https://doi.org/10.1016/j.cageo.2013.12.015

Wen, S., & Rose, W. I. (1994). Retrieval of sizes and total masses of particles in volcanic clouds using AVHRR bands 4 and 5. *Journal of Geophysical Research*, *99*(D3), 5421–5431. https://doi.org/10.1029/93JD03340

Wilson, L., & Self, S. (1980). Volcanic explosion clouds: Density, temperature, and particle content estimates from cloud motion. *Journal of Geophysical Research*, *85*(B5), 2567–2572. https://doi.org/10.1029/JB085iB05p02567

Wilson, L., & Walker, G. P. L. (1987). Explosive volcanic eruptions - VI. Ejecta dispersal in plinian eruptions: The control of eruption conditions and atmospheric properties. *Geophysical Journal International*, *89*(2), 657–679. https://doi.org/10.1111/j.1365-246X.1987.tb05186.x

Woodhouse, M. J., Hogg, A. J., Phillips, J. C., & Sparks, R. S. J. (2013). Interaction between volcanic plumes and wind during the 2010 Eyjafjallajökull eruption, Iceland. *Journal of Geophysical Research: Solid Earth*, *118*(1), 92–109. https://doi.org/10.1029/2012JB009592

Woodhouse, M. J., Phillips, J. C., & Hogg, A. J. (2016). Unsteady turbulent buoyant plumes. *Journal of Fluid Mechanics*, *794*, 595–638. https://doi.org/10.1017/jfm.2016.101

Woods, A. W. (1988). The fluid dynamics and thermodynamics of eruption columns. *Bulletin of Volcanology*, *50*(3), 169–193. https://doi.org/10.1007/BF01079681

Yu, T., Rose, W. I., & Prata, A. J. (2002). Atmospheric correction for satellite-based volcanic ash mapping and retrievals using "split window" IR data from GOES and AVHRR. *Journal of Geophysical Research*, *107*(D16), 4311. https://doi.org/10.1029/2001JD000706